
A COMPARISON OF ATMOSPHERIC CORRECTION METHODS ON HYPERION IMAGERY IN FOREST AREAS

Mufit CETIN *
Nebiyе MUSA OGLU **
Osman Hilmi KOCAL *

Received: 26.02.2016; revised: 05.12.2016; accepted: 28.02.2017

Abstract: The reflectance values recorded by Earth observing satellite sensors can be different from the surface reflectance values measured on the ground due to interference of gases and water vapor in the atmosphere. Therefore, atmospheric correction is a significant procedure to derive the true surface reflectance value during the processing of remotely sensed imagery especially with hyperspectral data. In this context, this study attempts to analyze the quality of the surface reflectance derived from EO-1 Hyperion hyperspectral imagery using the atmospheric radiative transfer (RT) models (FLAASH and ATCOR) and empirical line (EL) method. In the study, ground-based reflectance measurements derived from ASD FieldSpec spectroradiometer are used as reference to evaluate the quality of the retrieved surface reflectance. The results showed that EL and ATCOR methods achieved the best results for reducing some of the atmospheric effects, but FLAASH method resulted in strong anomalies in the corrected reflectance.

Keywords: Satellite Image, Hyperspectral, Hyperion, Atmospheric Correction.

HYPERION Görüntüsü ile Atmosferik Düzeltme Yöntemlerinin Karşılaştırılması: Orman Alanı Örneği

Öz: Uzaktan algılama amaçlı algılayıcılar tarafından elde edilen yansıma değerleri atmosferik etkilerden dolayı hatalar içermektedir. Dolayısıyla, özellikle hiperspektral uydu görüntülerinin işlenmesinde ve analizinde doğru sonuçlar elde edilmesi için atmosferik düzeltme önemli bir işlemdir. Bu kapsamda, EO-1 Hyperion hiperspektral uydu görüntüsü kullanılarak atmosferik ışınım transfer modelleri (FLAASH, ATCOR) ve Doğrusal Ampirik (EL) yöntemi kullanılarak performans sonuçları sunulmuştur. Elde edilen düzeltilmiş verilerin kalite analizi ASD spektrometre aleti ile yapılan yer ölçmeleri kullanılarak gerçekleştirilmiştir. Çalışmada elde edilen sonuçlara göre EL ve ATCOR yöntemlerinin atmosferik etkinin giderilmesinde en iyi sonuçları verdiği, FLAASH yönteminin ise düzeltilmiş reflektans eğrilerinde güçlü sapmalara neden olduğu görülmüştür.

Anahtar Kelimeler: Uydu görüntüsü, Hiperspektral, Hyperion, Atmosferik düzeltme.

1. INTRODUCTION

Spaceborne remote sensing is an efficient and relatively inexpensive way as compared to the conventional ground-based methods for the mapping of land covers, especially at regional and national levels. Hyperspectral imaging, which is one of the technological developments in remote sensing, opens new possibilities to detect particular types of earth surface materials. The hyperspectral systems generate hundreds of discrete, contiguous spectral narrow bands than the

* Yalova University, Department of Computer Engineering, Tigem Campus Yalova, 77200, TURKEY

** Istanbul Technical University, Department of Geomatic Engineering, Maslak/Istanbul, 34469, TURKEY

Correspondence Author: Mufit Cetin (mufit.cetin@yalova.edu.tr)

multispectral sensors which are most commonly used in remote sensing applications. For that reason, hyperspectral remote sensing has wide range of scientific and technical applications in forestry, agriculture, geology and environmental management such as mineral exploration, predictions of crop yield, detection of vegetation stress and soil mapping (Hardin and Hardin, 2013; Shang and Chisholm, 2014; Lee and others, 2014; Schmid and others, 2016).

Using of raw hyperspectral satellite images directly is not very convenient to retrieve reflectance values of the ground materials in the specific applications of remote sensing due to atmospheric effects and sensor sensitivity. Therefore, radiometric calibration and atmospheric correction are significant procedures to create a consistent surface reflectance from the hyperspectral data (Guanter and others, 2007a). A number of atmospheric correction methods have been developed based on radiative transfer codes (i.e. LOWTRAN and MODTRAN) in literature such as ATREM (Gao and others,1993), FLAASH (Matthew and others, 2000), ACORN (Miller, 2002), HATCH (Qu and others, 2003) and ATCOR (Richter, 1996). Various studies are conducted to evaluate the performance of atmospheric correction methods for different remotely sensed images such as Landsat TM (Lu and others, 2002; Norjamäki and Tokola, 2007), AVIRIS (Airborne Visible/Infrared Imaging Spectrometer) (Farrand and others, 1994; Veraguth and others, 1995), IKONOS (Karpouzli and Malthus, 2003; Xu and Huang, 2008) and others (Dwyer and others, 1995; Perry and others, 2000).

In this study, both qualitative and quantitative spectral analysis on Hyperion imagery are implemented to compare three common methods including Empirical Line (EL), Atmospheric correction (ATCOR) and Fast Line-of-sight Atmospheric Analysis of Spectral Hypercubes (FLAASH). The field reflectance measurements are obtained from known locations simultaneously with an Analytical Spectral Devices (ASD) Fieldspec Pro spectroradiometer in order to perform the spectral quality analysis of the methods. The results showed that EL and ATCOR methods achieved the best results for reducing some of the atmospheric effects, but FLAASH method is caused to strong anomalies in the corrected reflectance.

2. DATA

The study area is located in the forest belt of Eskisehir province at Northwest of Interior Anatolia region in Turkey (Figure 1). The spectral fields measurements are implemented with the ASD instrument cover the wavelength range of 350 to 2500 nm. The spectral measurements are collected with a 25° FOV's at Sundiken Mountain between September 16th and 17th 2004 in clear sky.



Figure 1:
Location of the study area

The spectral signatures are obtained from the ground surface between 11:00 and 14:00 on the same day as the satellite pass due to eliminate illumination effects. Also sample plots were selected from flat homogenous areas as 50 m × 50 m quadrants which are larger than one pixel in order to eliminate topographic effects (Cetin and Musaoglu, 2009). A total of six samples are

used in the study, including water, stubble field, pasture, one deciduous (oak) and two coniferous species (*Pinus sylvestris* and *Pinus nigra*).

The hyperspectral data were acquired by EO-1 Hyperion sensor on September 17, 2004, around 10:30 a.m. local time. EO-1 spacecraft has two types of optic sensors that include the Advanced Land Imager (ALI) and Hyperion. EO-1 satellite can collect both high-resolution panchromatic (PAN) and low-resolution multispectral (MS) images simultaneously by using ALI sensor and hyperspectral image gathered using Hyperion sensor. Hyperion scenes cover just about 7.7 km in the across-track direction, and 42 km in the along-track direction on the ground. The Hyperion image contains 242 channels ranging from 356 to 2577 nm in 10 nm spectral and 30 m spatial resolutions (Cetin and Musaoglu, 2009; Pearlman et al., 2003).

3. METHODOLOGY

The methodology for retrieving reflectance spectra from Hyperion imagery consists of the following three main steps including radiometric, geometric and atmospheric corrections. The radiometric errors such as destriping and smile effects generally occur in the Hyperion dataset due to the internal effects of the sensor such as miscalibration of the detector and noise of the system. All the methodological steps are illustrated in Figure 2.

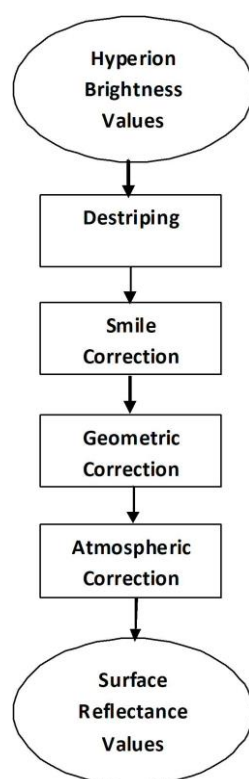


Figure 2:
The flow diagram for retrieval of surface reflectance values.

3.1. Radiometric Correction

3.1.1. Exclusion of Bad Bands

EO-1 Hyperion Level 1 Radiometric product contains only 198 calibrated bands include 8-57 for the VNIR and 77-224 for the SWIR due to the detectors' low responsivity. Band 56

(915.23 nm) and band 57 (925.41 nm) in VNIR with band 77 (912.45 nm) and band 78 (922.54 nm) in SWIR are overlapped. Only 196 unique channels remained when un-calibrated bands with band 77 and 78 are removed. Water absorption bands in 1340-1450 nm and 1750-1970 nm are eliminated. In this study, the EO-1 Hyperion image is visually inspected band by band to eliminate spectral channels whose signals were significantly affected by atmospheric absorption windows and low signal to noise ratio (Christian and Krishnayya, 2007). The defective bands are excluded 1-7, 58-78, 119 – 130, 164 – 186, and 217 – 224, namely and 153 healthy bands are remained for analysis (Table 1). EO-1 Hyperion Level 1R product include some sensor related artifacts such as vertical striping and smile effects are corrected before image fusion (Goodenough and others, 2003).

Table 1. The spectral bands used in the Hyperion data sets

Detectors	Bands	Wavelength (nm)	Number of bands
VNIR	8–57	426 – 926	50
SWIR	79 – 118	933 – 1326	40
	131 – 163	1457 – 1780	33
	187 – 216	2022 – 2315	30
Total used bands			153

3.1.2. Destriping

Vertical-striping is usually occurs in the image acquired using pushbroom sensors such as Airborne Visible/Infrared Imaging Spectrometer and Hyperion due to various effects such as detector nonlinearities, movement of the slit with respect to the focal plane and temperature effects (Kruse and others, 2003). First, vertical stripes should be removed before the analysis of the Hyperion image and eliminated to provide accurate radiometric calibration (Goetz and others, 2003). Therefore, the mean of each column per image was calculated and the quality control is performed by inspecting visually.

3.1.3. Smile Correction

The spectral shift errors caused by the large spectral artifacts in the atmospheric absorption regions. A spectral shift in the size of 0.1 nm for the band center with Full Width at Half Maximum (FWHM) of 10 nm can be caused to 5% difference in the reflectance values (Goetz and others, 2003; Guanter and others, 2007b). Moreover, some studies showed that the spectral shift errors can reach up to 20% in the NIR region and 50% in the atmospheric absorption bands close to 1400 and 1900 nm due to strong water vapor absorption (Cocks and others, 1998; Guanter and others, 2006). Prior to atmospheric correction, this spectral shift effect has to be corrected to retrieve the proper surface reflectance values. Therefore, a weighted linear interpolation method is performed on each column of the hyperspectral data using the auxiliary spectral calibration table (smile table), extracted from the header file of Level 1R product.

The "weighted linear interpolation" can be thought as "moving linear interpolation" in spectral direction, which is performed with the following formula:

$$d = [d(i + 1) - d(i)] * [w - w(i)]/[w(i + 1) - w(i)] + d(i) \quad (1)$$

where d is the real DN at the nominal band centre wavelength w , which is in header file;

$d(i)$ is the DN at wavelength $w(i)$, which is in smile table;

$d(i+1)$ is the DN at wavelength $w(i+1)$, which is in smile table. w is usually between $w(i)$ and $w(i+1)$.

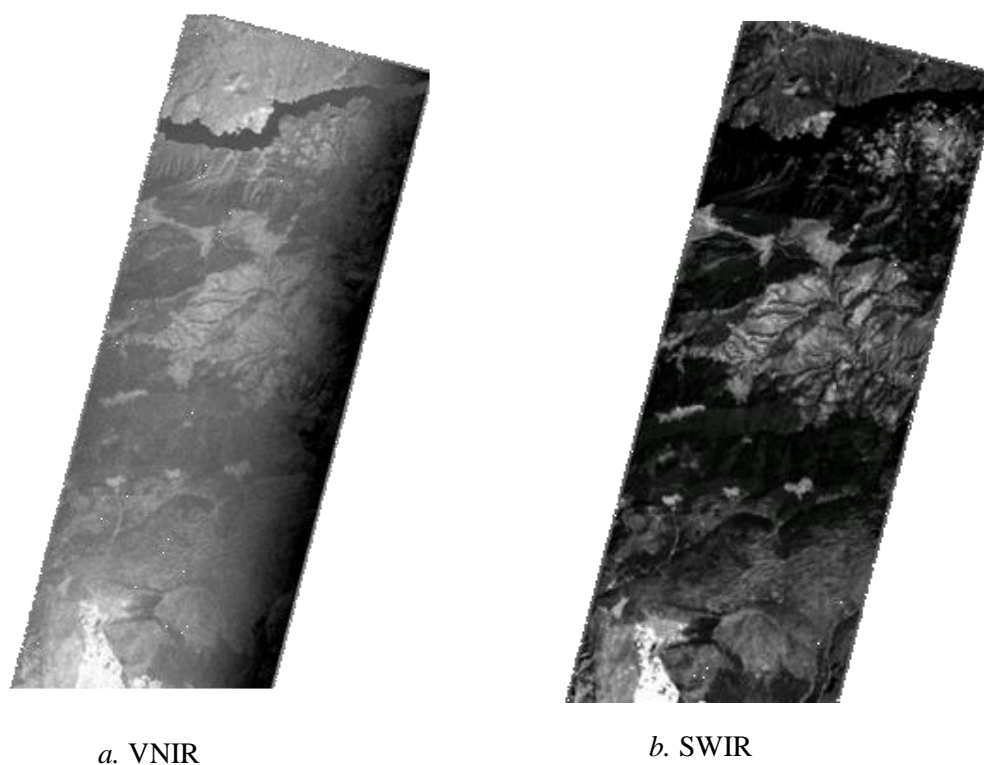


Figure 3:
MNF band 1 of VNIR and SWIR bands, corrected spectral curvature effects (smile)

Figure 3 shows minimum noise fraction (MNF) transform of VNIR bands. First MNF band represents brightness gradients due to smile effect for Hyperion images. On the other hand, this brightness gradient is not observed in the SWIR region. Hyperion data, applied for the weighted linear interpolation to reduce the smile effects, is examined in MNF space to evaluate the smile correction results. But the results show that improved imagery still contains cross-track brightness gradients.

3.2. Geometric Correction

Firstly, Hyperion imagery is orthorectified by using digital elevation model (DEM) created from 1:25 000 scaled topographic maps, with 19 Ground Control Points (GCPs) and 7 Independent Check Points (ICPs). The Root Mean Square (RMS) residuals of the GCPs are 0.39 pixels in X, 0.40 pixels in Y directions and 0.55 pixels in total, respectively. The RMS errors of the ICPs are 0.37 pixels, 0.58 pixels and 0.69 pixels in X, Y directions and in total, respectively. The nearest neighbor resampling method is used to preserve the original values in the image rectification (Cetin and Musaoglu, 2009).

3.3. Atmospheric Correction

The main objective of atmospheric correction methods is to reduce atmospheric effects in order to retrieve more accurate surface reflectance values from the satellite images. Methods can be divided into two broad categories including relative and absolute techniques. Also, the relative atmospheric correction method consists of three sub-groups include flat field method, internal average relative reflectance model and empirical line method. Relative atmospheric correction methods utilize some statistical information extracted from images and priori

knowledge of the ground surfaces obtained from field measurements. On the other hand, the absolute atmospheric correction methods needs some inputs such as solar geometry (azimuth, elevation), sensor geometry (zenith, azimuth), scene centre location, aerosol model (rural, urban, etc), atmospheric condition and time of image acquisition. Therefore, each of the atmospheric correction methods has their own benefits and challenges according to the aim and opportunities of the research (Gao and others, 1993; Guanter and others, 2007a; Mahiny and Turner, 2007; Cetin and Musaoglu, 2008; San and Suzen, 2010).

3.3.1.1. Empirical Line Method

This method suggest that there is linear relationship between the spectral radiance values observed by the sensor and the spectral reflectance values obtained from the ground field spectrometer for each of the calibration objects within each band of the remotely sensed image. Atmospherically corrected images can be produced applying this extracted linear relationship to remotely sensed data (Smith and Milton, 1999). The EL method is based on the the linear regression model as follows:

$$L_i(\lambda) = \rho(\lambda) \cdot \beta_i + \alpha_i \quad (2)$$

where $L_i(\lambda)$ is the spectral radiance for a given pixel in spectral band i , $\rho(\lambda)$ is the reflectance value of the sample, β_i and α_i coefficients are slope and intercept derived from band i by the linear regression model, respectively.

The coefficients can be determined by using the Eq.(2). Field measurements of calibration objects are the most important stage to obtain the valid and accurate results in EL method. The field measurements of the calibration objects have to be done at the same time with satellite overpass. This method assumes that all study area has the same atmospheric conditions and no topographic effect. Besides, selected sample areas should be flat, homogeneous and a few pixels in size. Various studies are conducted to calibrate remotely sensed data using empirical line method especially for broad band images (Farrand and others, 1994; Karpouzli and Malthus, 2003; Xu and Huang, 2008). As in many atmospheric calibration studies in the literature, the water and stubble sample areas as the dark and light calibration targets for spectral calibration depending on the number of selected samples. Thus, the linear equation is used to predict the reflectance of other targets on the image. Moreover, additional field spectral measurements are carried out to evaluate the performance of the atmospheric correction methods.

3.3.1.2. Radiative Transfer Models

It can be modeled using the radiative transfer codes to reduce the scattering, water vapor absorptions and transmission properties of the atmosphere without field measurements or priori knowledge. In literature, radiative transfer models are more commonly used than the relative correction techniques (especially flat field and internal average relative reflectance) since they provide more accurate results (Goetz and others, 2002). Radiative transfer models are based on the following simple expression:

$$L_c(\lambda) = L_s(\lambda) - L_p(\lambda) \quad (3)$$

where $L_s(\lambda)$ the radiance value is acquired by a sensor, $L_p(\lambda)$ is the atmospheric path radiance computed by radiative transfer model and $L_c(\lambda)$ is corrected radiance value for a given pixel in the satellite image.

In this study, ATCOR and FLAASH atmospheric models, based on MODTRAN-4 radiative transfer code, are used to evaluate the results of the corrected images using the field spectral measurements and to compare with relative atmospheric methods. For accomplishing this, we have inserted some parameters to the model that include sensor altitude, wavelength date, Full Width Half Maximum (FWHM), time, season, latitude/longitude of study area,

average elevation etc. A FLAASH atmospheric correction model developed to eliminate atmospheric effects by the Air Force Phillips Laboratory (Adler-Golden and others, 1999). It provides accurate surface reflectance values using the atmospheric parameters (Felde and others, 2003) ATCOR model have been developed by Dr. Richter of the German Aerospace Center in the last decade. ATCOR model has several different sub-models include ATCOR-2, ATCOR-3, ATCOR-4 and ATCOR Thermal. It is used ATCOR-2 in nearly flat terrain, ATCOR-3 in mountainous terrain. ATCOR-4 is utilized for airborne remotely sensed images. Moreover, ATCOR model can provide the atmospheric correction for thermal images (Richter, 1996).

4. RESULTS

The surface reflectance values retrieved from atmospheric correction methods, which are applied to a Hyperion image, are compared with simultaneously acquired field spectral measurements obtained by an ASD spectrometer for each sample and performed quantitative analysis to assess the performance of the atmospheric correction methods. Spectral regions around 1450 nm, 1950 nm and 2500 nm have been excluded from the evaluation because of the strong water vapor and atmospheric gases.

4.1. Visual Analysis

Figure 4 shows that the spectral matching between the retrieved and ground field reflectance spectra of the sample objects which are considerably better for EL and ATCOR models at many wavelengths.

The calculated reflectance values at the spectral regions which do not have strong atmospheric absorption features are within one standard deviation of the ground reflectance. But, there are some anomalies in some parts of SWIR regions. Moreover, the calculated reflectance values for all samples at visible wavelengths are very close to the ground reflectance. The differences in spectral behaviors are remarkable in the atmospheric absorption bands due to water vapor and atmospheric gaseous especially around 940 nm, 960 nm, 1100nm and 1200 nm for FLAASH and EL methods. In particularly, FLAASH model shows the most sensitivity and significant anomalies in some spectral bands of Hyperion data due to the strong atmospheric effects and low signal to noise ratio.

To provide an accurate comparison between field and retrieved surface spectra, the natural conditions of field measurements can not be the same as the satellite sensing because IFOV is different for both systems. For that reason, the spectral curves of vegetations including oak and pine samples retrieved by ground field measurements is noticeably shifted from all atmospheric correction models in the NIR and SWIR spectral region due to the natural variability of samples such as the background soil reflectance and angular effects in vegetated areas. But, there is a good agreement between the ground field and corrected spectral curves for the pasture, stubble and water samples. As a result of the visual evaluation, EL and ATCOR models applied on the Hyperion data generated more similar to ground truth spectra and smoother spectral curves of the collected samples than FLAASH model in all spectral regions.

4.2. Statistical Analysis

The performance of the atmospheric correction algorithms for Hyperion data is examined using a number of different statistical indexes to increase the robustness of quantitative assessment and to measure the similarity between the field spectra and the retrieved spectra for each sample at the same location. The principles of statistical metrics including Correlation Coefficient (CC), Root Mean Square Error (RMSE), Spectral Feature Fitting (SFF) and Spectral Angle Mapper (SAM) are briefly presented as follows.

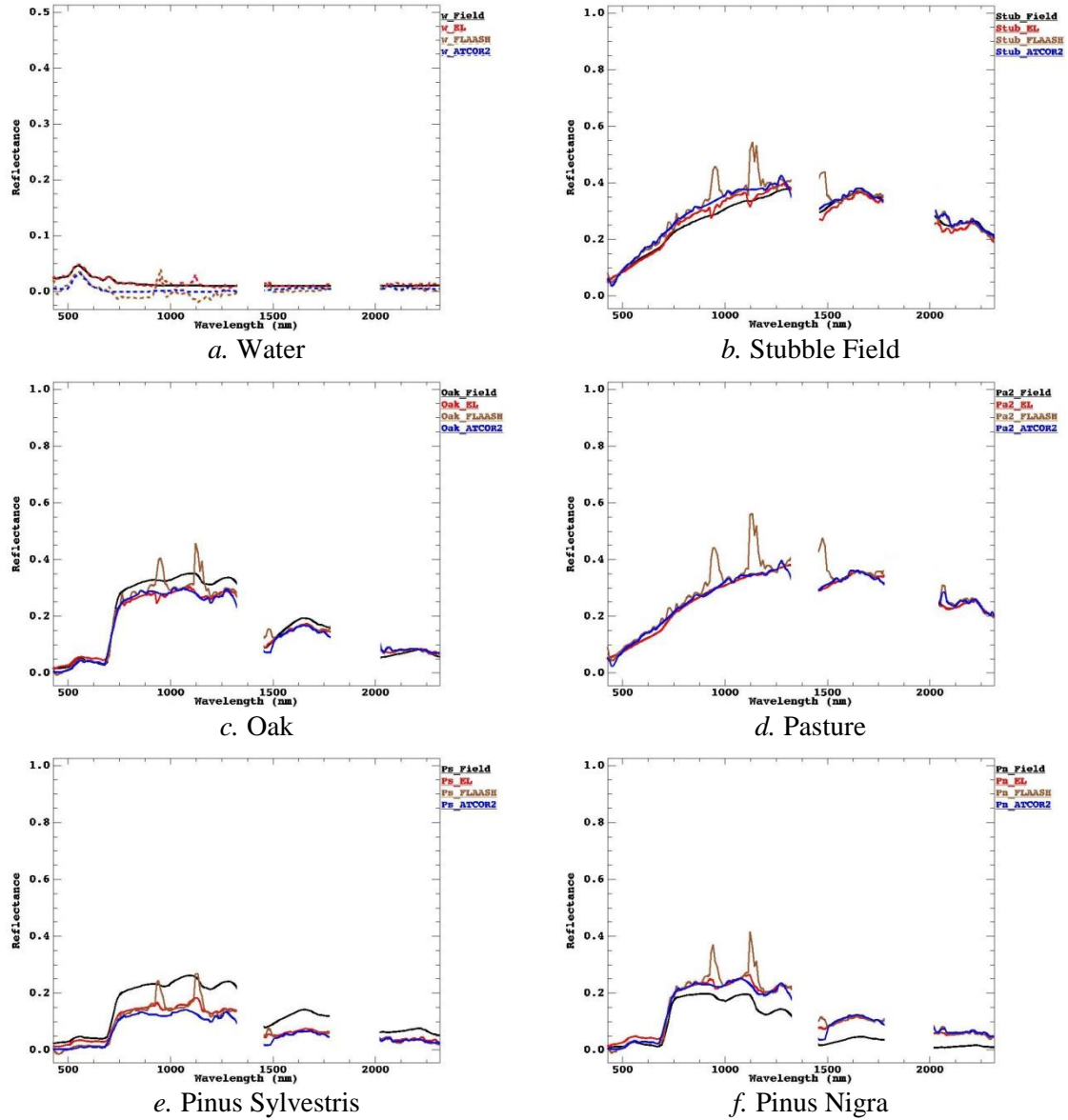


Figure 4:
Spectral curves of the samples obtained from ground field (black) and corrected Hyperion image using EL (red), FLAASH (brown) and ATCOR (blue) models.

CC is the correlation between the reference spectra and the retrieved spectra. It shows the similarity between each other. It should be as close as to 1.

RMSE, as defined below, are calculated from the reference field and retrieved spectra in each sample. The RMSE should be as low as possible (Wald, 2000; Wang, 2004).

$$RMSE_k = \frac{1}{n} \sqrt{\sum_{i=1}^n [V_{0k}(i) - V_{fk}(i)]^2} \quad (4)$$

In the above formula, n is the number of bands of the retrieved spectra, V_{0k} and V_{fk} are the reflectance values of the k th band of the reference and the retrieved spectra for each sample, respectively.

Spectral Feature Fitting (SFF) utilizes the specific absorption features in spectra for both the reference and the unknown materials. This technique provides direct identification of unknown materials comparing the band depths of the both spectrum. The root-mean-square (RMS) error between the unknown and the reference spectra is calculated using the least-squares-fitting model. A lower RMS value indicates a better match of the unknown to the reference (Clark and others, 2003).

Spectral Angle Mapper (SAM) indicates the spectral angle between the reference and the retrieved spectra for each sample (Wang, 2005). A value of SAM that is close to zero shows the similarity of two spectra and it is measured in radians.

$$SAM = \arccos \left(\frac{\sum_{k=1}^N (Vo_k \cdot Vf_k)}{\sqrt{\sum_{k=1}^N (Vo_k)^2 \cdot \sum_{k=1}^N (Vf_k)^2}} \right) \quad (5)$$

N is the number of bands, Vo_k and Vf_k are the reflectance values of the k th band of the reference and the retrieved spectra, respectively.

The results in Table 2 show that correlation coefficients of all methods are higher than 0.90 except ATCOR and FLAASH methods for water sample due to water absorption bands in the 940 nm and 1200 nm. At the same time, the RMSE values of EL method are lowest for water, stubble and pasture sample areas; but FLAASH method has low quality. Besides, SFF and SAM values for FLAASH method represent low performances than others. Especially SFF and SAM values retrieved from all samples indicate that EL method for the Hyperion data is slightly better than to ATCOR method.

Results of spectral quality assessment techniques include visual and statistical analysis for the Hyperion imagery show that EL method generally has better performance than ATCOR and FLAASH methods in all types of objects. Besides, FLAASH method yielded poor results than other methods. Furthermore, the results indicate that there is consistently good agreement between visual and statistical comparison of the atmospheric methods.

Table 2: Results of CC, RMSE, SFF and SAM statistical parameters for ground and corrected image spectral reflectance from ATCOR, FLAASH and EL atmospheric models.

	CC			RMSE			SFF			SAM		
	EL	ATCOR	FLAASH	EL	ATCOR	FLAASH	EL	ATCOR	FLAASH	EL	ATCOR	FLAASH
Water	0.94	0.77	0.64	0.0003	0.0006	0.0013	0.897	0.889	0.852	0.173	0.588	1.099
Stubble	0.98	0.94	0.92	0.0014	0.0030	0.0042	0.978	0.959	0.950	0.060	0.065	0.131
Pasture	1.00	0.92	0.92	0.0002	0.0039	0.0041	0.991	0.941	0.933	0.007	0.054	0.137
Oak	1.00	0.97	0.97	0.0027	0.0027	0.0027	0.953	0.908	0.846	0.069	0.075	0.128
P. Nigra	0.97	0.95	0.93	0.0026	0.0022	0.0043	0.885	0.802	0.784	0.242	0.246	0.258
P. Sylvestris	0.99	0.93	0.92	0.0015	0.0024	0.0049	0.924	0.917	0.841	0.087	0.110	0.230

Note: The results are ranked using the three colors as normal (red), good (yellow) and better (green).

5. CONCLUSION

Surface reflectance spectra for various samples retrieved with EL, ATCOR and FLAASH methods from Hyperion image is compared with simultaneously collected ground measurements by ASD field spectrometer. As can be seen in the graphical plots and statistical quantitative results among three models, EL and ATCOR methods achieved the best results for

reducing some of the atmospheric effects required for hyperspectral image processing. Besides, EL method has slightly better performance than ATCOR as shown by the statistical analysis. As a conclusion, we observe that the atmospheric correction is a significantly important procedure for the hyperspectral image analysis of forest areas. Furthermore, the results of spectral quality analysis also show the importance of selecting appropriate methods to correct the atmospheric effects on the hyperspectral images such as EO-1 Hyperion and CHRIS Proba.

REFERENCES

1. Adler-Golden, S.M., Matthew, M.W., Bernstein, L.S., Levine, R.Y., Berk, A., Richtsmeier, S.C., Acharya, P.K., Anderson, G.P., Felde, G., Gardner, J., Hike, M., Jeong, L.S., Pukall, B., Mello, J., Ratkowski, A. and Burke, H.H. (1999) Atmospheric correction for shortwave spectral imagery based on MODTRAN4, *SPIE Proc. Imaging Spectrometry*, 61-69. doi:10.1117/12.366315
2. Cetin, M. and Musaoglu, N. (2008). Spectral calibration and atmospheric correction of Hyperion images, *2th Remote Sensing and GIS Symposium*, Kayseri, Turkey, October, Proc. no:60. (In Turkish)
3. Cetin, M. and Musaoglu, N. (2009) Merging hyperspectral and panchromatic image data: qualitative and quantitative analysis, *Int. J. Remote Sens.*, 30(7), 1779–1804. doi:10.1080/01431160802639525
4. Christian, B. and Krishnaya, N. S. R. (2007) Spectral signatures of teak (*Tectona grandis* L.) using hyperspectral (EO-1) data, *Current Science*, 93(9), 1291-1296.
5. Clark, R.N., Swayze, G.A., Livo, K.E., Kokaly, R.F., Sutley, S.J., Dalton, J.B., McDougal, R.R. and Gent, C.A. (2003) Imaging spectroscopy: Earth and planetary remote sensing with the USGS Tetracorder and expert systems, *Journal of Geophysical Research*, 108(E12), 5.1-5.44. doi:10.1029/2002JE001847
6. Cocks, T., Jenssen, R., Stewart, A., Wilson, I. and Shields, T. (1998) The hymap airborne hyperspectral sensor: The system, calibration and performance, *Proc. of the First EARSeL Workshop on Imaging Spectroscopy*, Zurich, Switzerland, 37–42.
7. Dwyer, J.L., Kruse, F.A. and Lefkoff, A.B. (1995) Effects of empirical versus model based reflectance calibration on automated analysis of imaging spectrometer data: A case study from the Drum Mountains, Utah, *Photogrammetric Engineering and Remote Sensing*, 61(10), 1247–1254.
8. Felde, G.W., Anderson, G.P., Cooley, T.W., Matthew, M.W., Adler-Golden, S.M., Berk, A., and Lee, J. (2003) Analysis of Hyperion Data with the FLAASH Atmospheric Correction Algorithm, *IEEE Geoscience and Remote Sensing Symposium*, 2003, 1, 90–92. doi: 10.1109/IGARSS.2003.1293688
9. Farrand, W.H., Singer, R.B. and Merenyi, E. (1994) Retrieval of apparent surface reflectance from AVIRIS data: A comparison of empirical line, radiative transfer, and spectral mixture methods, *Remote Sensing of Environment*, 47(3), 311–321. doi: 10.1016/0034-4257(94)90099-X
10. Gao, B.C., Heidebrecht, K.B. and Goetz, A.F.H. (1993) Derivation of scaled surface reflectances from AVIRIS data, *Remote Sensing of Environment*, 44(2-3), 165-178. doi:10.1016/0034-4257(93)90014-O
11. Goetz, A., Ferri, M., Kindel, B., and Qu, Z. (2002) Atmospheric Correction of Hyperion Data and Techniques for Dynamic Scene Correction, *Proc. International Geoscience and Remote Sensing Symposium (IGARSS)*, 1408–1410. doi: 10.1109/IGARSS.2002.1026132

12. Goetz, A.F.H., Kindel, B.C., Ferri M. and Qu, Z. (2003) HATCH: Results from simulated radiances, AVIRIS and HYPERION, *IEEE Transactions on Geoscience and Remote Sensing*, 41(6/1), 1215–1221. doi: 10.1109/TGRS.2003.812905
13. Goodenough, D.G., Dyk, A., Niemann, O., Pearlman, J.S., Chen, H., Han, T., Murdoch, M., and West, C. (2003) Processing HYPERION and ALI for Forest Classification, *IEEE Trans. Geosci. Remote Sensing*, 41(6/1), 1321-1331. doi: 10.1109/TGRS.2003.813214
14. Guanter, L., Richter, R. and Moreno, J. (2006) Spectral calibration of hyperspectral imagery using atmospheric absorption features, *Applied Optics*, 45(10), 2360–2370. doi: 10.1364/AO.45.002360
15. Guanter, L., Estellés, V. and Moreno, J. (2007a) Spectral calibration and atmospheric correction of ultra-fine spectral and spatial resolution remote sensing data. Application to CASI-1500 data, *Remote Sensing of Environment*, 109(1), 54–65. doi:10.1016/j.rse.2006.12.005
16. Guanter, L., Gonzalez-Sanpedro, M., Del, C. and Moreno, J. (2007b) A method for the atmospheric correction of ENVISAT/MERIS data over land targets, *International Journal of Remote Sensing*, 28(3-4), 709–728. doi: 10.1080/01431160600815525
17. Hardin, P. and Hardin, A. (2013) Hyperspectral remote sensing of urban areas, *Geography Compass*, 7(1), 7-21. doi: 10.1111/gec3.12017
18. Karpouzli, E. and Malthus, T. (2003) The empirical line method for the atmospheric correction of IKONOS imagery, *International Journal of Remote Sensing*, 24(5), 1143–1150. doi: 10.1080/0143116021000026779
19. Kruse, F.A., Boardman, J.W. and Huntigton, J.F. (2003) Comparison of airborne hyperspectral data and EO-1 Hyperion for mineral mapping, *IEEE Transactions on Geoscience and Remote Sensing*, 41(6), 1388-1400. doi: 10.1109/TGRS.2003.812908
20. Lee, M., Huang, Y., Yao, H., Thomson, S.J. and Bruce, L. (2014) Determining the Effects of Storage on Cotton and Soybean Leaf Samples for Hyperspectral Analysis. *IEEE Journal of Selected Topics in Applied Earth Observations and Remote Sensing*, 7(6). doi:10.1109/JSTARS.2014.2330521
21. Lu, D., Mausel, P., Brondizio, E., and Moran, E. (2002) Assessment of atmospheric correction methods for Landsat TM data applicable to Amazon basin LBA research, *International Journal of Remote Sensing*, 23(13), 2651–2671. doi: 10.1080/01431160110109642
22. Mahiny, A.S. and Turner, B.J. (2007) A Comparison of Four Common Atmospheric Correction Methods, *Photogrammetric Engineering & Remote Sensing*, 73(4), 361-368. doi: 10.14358/PERS.73.4.361
23. Matthew, M.W., Adler-Golden, S.M., Berk, A., Richtsmeier, S.C., Levine, R.Y., Bernstein, L.S., Acharya, P.K., Anderson, G.P., Felde, G.W., Hoke, M.P., Ratkowski, A., Burke, H.-H., Kaiser, R.D. and Miller, D.P. (2000) Status of Atmospheric Correction Using a MODTRAN4-based Algorithm, *Proc. SPIE Algorithms for Multispectral, Hyperspectral and Ultraspectral Imagery VI*, 199-207. doi:10.1117/12.410341
24. Miller, C.J. (2002) Performance assessment of ACORN atmospheric correction algorithm, *Proc. SPIE Algorithms and Technologies for Multispectral, Hyperspectral and Ultraspectral Imagery VIII*, 438–449. doi: 10.1117/12.478777
25. Norjamäki, I. and Tokola, T. (2007) Comparison of Atmospheric Correction Methods in Mapping Timber Volume with Multitemporal Landsat Images in Kainuu, Finland,

- Photogrammetric Engineering and Remote Sensing*, 73(2), 155-164. doi: 10.14358/PERS.73.2.155
26. Pearlman, J.S., Barry, P.S., Segal, C.C., Shepanski, J., Beiso, D. and Carman, S.L. (2003) Hyperion, a Space-Based Imaging Spectrometer, *IEEE Transactions on Geoscience and Remote Sensing*, 41(6), 1160-1173. doi: 10.1109/TGRS.2003.815018
 27. Perry, E.M., Warner, T. and Foote, P. (2000) Comparison of atmospheric modeling versus empirical line fitting for mosaicking HYDICE imagery, *International Journal of Remote Sensing*, 21(4), 799–803. doi:10.1080/014311600210588
 28. Qu, Z., Kindel, B.C. and Goetz, A.F.H. (2003) The high accuracy atmospheric correction for hyperspectral data (HATCH) model, *IEEE Transactions on Geoscience and Remote Sensing*, 41(6/1), 1223–1231. doi:10.1109/TGRS.2003.813125
 29. Richter, R. (1996) Atmospheric correction of satellite data with haze removal including a haze/clear transition region, *Computers and Geosciences*, 22(6), 675–681. doi:10.1016/0098-3004(96)00010-6
 30. San, B.T. and Suzen, M.L. (2010) Evaluation of different atmospheric correction algorithms for EO-1 Hyperion Imagery, *ISPRS Technical Commission VII Symposium*, Kyoto, JAPONYA, 38(8), 392-397.
 31. Schmid, T., Rodriguez-Rastrero, M., Escribano, P., Palacios-Orueta, A., Ben-Dor, E., Plaza, A., Milewski, R., Huesca, M., Bracken, A., Ciuendez, V., Pelayo, M., Chabrillat, S. (2016) Characterization of soil erosion indicators using hyperspectral data from a Mediterranean rainfed cultivated region, *IEEE J. Sel. Topics Appl. Earth Observ. Remote Sens.*, 9(2), 845-860. doi: 10.1109/JSTARS.2015.2462125
 32. Shang, S. and Chisholm, L.A. (2014) Classification of Australian native forest species using hyperspectral remote sensing and machine-learning classification algorithms, *IEEE J. Sel. Topics Appl. Earth Observ. Remote Sens.*, 7(6), 2481-2489. doi: 10.1109/JSTARS.2013.2282166
 33. Smith, G.M. and Milton, E.J. (1999) The use of the empirical line method to calibrate remotely sensed data to reflectance, *International Journal of Remote Sensing*, 20(13), 2653–2662. doi: 10.1080/014311699211994
 34. Veraguth, S., Keller, J., Schaepman, M. and Itten, K.I. (1995) Atmospheric correction of AVIRIS imagery in Central Switzerland. Sensitivity analysis regarding correction methods, radiation transfer models and atmospheric profiles, *Proc. International Geoscience and Remote Sensing Symposium (IGARSS)*, 2069-2071. doi:10.1109/IGARSS.1995.524110
 35. Wald, L. (2000) Quality of high resolution synthesised images: Is there a simple criterion?. *Proceedings of the third conference "Fusion of Earth data: merging point measurements, raster maps and remotely sensed images"*, Sophia Antipolis, France, 99-103.
 36. Wang, Z., Bovik, A.C., Sheikh, H.R. and Simoncelli, E.P. (2004) Image quality assessment: From error visibility to structural similarity, *IEEE Trans. Image Process.*, 13(4), 600-612. doi: 10.1109/TIP.2003.819861
 37. Wang, Z., Ziou, D., Armenakis, C., Li, D. and Li, Q. (2005) A comparative analysis of image fusion methods, *IEEE Trans. Geosci. Remote Sens.*, 43(6), 1391-1402. doi: 10.1109/TGRS.2005.846874
 38. Xu, J.F. and Huang, J.F. (2008) Empirical Line Method Using Spectrally Stable Targets to Calibrate IKONOS Imagery, *Pedosphere*, 18(1), 124-130. doi:10.1016/S1002-0160(07)60110-6